

**Batched computation of the singular value
decompositions of order two by the AVX-512 vectorization**

Vedran Novaković*

*completed a major part of this research as a collaborator on the MFBDA project
10000 Zagreb, Croatia*

Received (received date)

Revised (revised date)

ABSTRACT

In this paper a vectorized algorithm for simultaneously computing up to eight singular value decompositions (SVDs, each of the form $A = U\Sigma V^*$) of real or complex matrices of order two is proposed. The algorithm extends to a batch of matrices of an arbitrary length n , that arises, for example, in the annihilation part of the parallel Kogbetliantz algorithm for the SVD of a square matrix of order $2n$. The SVD algorithm for a single matrix of order two is derived first. It scales, in most instances error-free, the input matrix A such that its singular values Σ_{ii} cannot overflow whenever its elements are finite, and then computes the URV factorization of the scaled matrix, followed by the SVD of a non-negative upper-triangular middle factor. A vector-friendly data layout for the batch is then introduced, where the same-indexed elements of each of the input and the output matrices form vectors, and the algorithm's steps over such vectors are described. The vectorized approach is then shown to be about three times faster than processing each matrix in isolation, while slightly improving accuracy over the straightforward method for the 2×2 SVD.

Keywords: batched computation; singular value decomposition; AVX-512 vectorization.

1. Introduction

Let a finite sequence $\mathbf{A} = (\mathbf{A}^{[k]})_k$, where $1 \leq k \leq n$, of complex 2×2 matrices be given, and let the corresponding sequences $\mathbf{U} = (\mathbf{U}^{[k]})_k$, $\mathbf{V} = (\mathbf{V}^{[k]})_k$ of 2×2 unitary matrices be sought for, as well as a sequence $\mathbf{\Sigma} = (\mathbf{\Sigma}^{[k]})_k$ of 2×2 diagonal matrices with the real and non-negative diagonal elements, such that $\mathbf{A}^{[k]} = \mathbf{U}^{[k]} \mathbf{\Sigma}^{[k]} (\mathbf{V}^{[k]})^*$, i.e., for each k , the right hand side of the equation is the singular value decomposition (SVD) of the left hand side. This batch of 2×2 SVD computational tasks arises naturally in, e.g., parallelization of the Kogbetliantz algorithm [1] for the $2n \times 2n$ SVD [2–4]. A parallel step of the algorithm, repeated until convergence, amounts to forming and processing such a batch, with each $\mathbf{A}^{[k]}$ assembled column by column

*e-mail address: venovako@venovako.eu<https://orcid.org/0000-0003-2964-9674>

from the elements of the iteration matrix at the suitably chosen pivot positions (p_k, p_k) , (q_k, p_k) , (p_k, q_k) , and (q_k, q_k) . The iteration matrix is then updated from the left by $(\mathbf{U}^{[k]})^*$ and from the right by $\mathbf{V}^{[k]}$, transforming the p_k th and the q_k th rows and columns, respectively, while annihilating the off-diagonal pivot positions.

For each k , the matrices $\mathbf{A}^{[k]}$, $\mathbf{U}^{[k]}$, $\mathbf{V}^{[k]}$, and $\mathbf{\Sigma}^{[k]}$ have the following elements,

$$\mathbf{A}^{[k]} = \begin{bmatrix} a_{11}^{[k]} & a_{12}^{[k]} \\ a_{21}^{[k]} & a_{22}^{[k]} \end{bmatrix}, \quad \mathbf{U}^{[k]} = \begin{bmatrix} u_{11}^{[k]} & u_{12}^{[k]} \\ u_{21}^{[k]} & u_{22}^{[k]} \end{bmatrix}, \quad \mathbf{V}^{[k]} = \begin{bmatrix} v_{11}^{[k]} & v_{12}^{[k]} \\ v_{21}^{[k]} & v_{22}^{[k]} \end{bmatrix}, \quad \mathbf{\Sigma}^{[k]} = \begin{bmatrix} \sigma_{\max}^{[k]} & 0 \\ 0 & \sigma_{\min}^{[k]} \end{bmatrix},$$

where $\sigma_{\max}^{[k]} \geq \sigma_{\min}^{[k]} \geq 0$. When its actual index k is either implied or irrelevant, $\mathbf{A}^{[k]}$ is denoted by A . Similarly, U , V , and Σ denote $\mathbf{U}^{[k]}$, $\mathbf{V}^{[k]}$, and $\mathbf{\Sigma}^{[k]}$, respectively, in such a case, and the bracketed indices of the particular elements are also omitted.

When computing in the machine's floating-point arithmetic, the real and the imaginary parts of the input elements are assumed to be rounded to finite (i.e., excluding $\pm\infty$ and **NaN**) **double** precision quantities, but the SVD computations can similarly be vectorized in single precision (**float** datatype in the C language [5]).

Let \mathbf{C} and \mathbf{W} denote the CPU's cache line size and the maximal SIMD width, both expressed in bytes, respectively. For an Intel CPU with the 512-bit Advanced Vector Extensions Foundation (AVX-512F) instruction set [6], $\mathbf{C} = \mathbf{W} = 64$. Let \mathbf{B} be the size in bytes of the chosen underlying datatype \mathbf{T} (here, $\mathbf{T} = \mathbf{double}$ in the real and the complex case alike, so $\mathbf{B} = 8$), and let $\mathbf{S} = \mathbf{W}/\mathbf{B} = 8$. If $n \bmod \mathbf{S} \neq 0$, let $\hat{n} = n + (\mathbf{S} - (n \bmod \mathbf{S}))$, else let $\hat{n} = n$.

This paper aims to show how to single-threadedly compute as many SVDs at the same time as there are the SIMD/vector lanes available (\mathbf{S}), one SVD by each lane. Furthermore, these vectorized computations can execute concurrently on the non-overlapping batch chunks assigned to the multiple CPU cores.

Techniques similar to the ones proposed in this paper have already been applied in [7] for vectorization of the Hari–Zimmermann joint diagonalizations of a complex positive definite pair of matrices [8] of order two, and could be, as future work, for the real variant of the Hari–Zimmermann algorithm for the generalized eigendecomposition [9] and the generalized SVD [10]. Those efforts do not use the C compiler intrinsics, but rely instead on the vectorization capabilities of the Intel Fortran compiler over data laid out in a vector-friendly fashion similar to the one described in section 3. Simple as it may seem, it is also a more fragile way of expressing the vector operations, should the compiler ever renegade on the present behavior of its autovectorizer. The intrinsics approach has been tried in [11] with 256-bit-wide vectors of the AVX2+FMA [6] instruction set, alongside AVX-512F, for vectorization of the eigendecompositions of symmetric matrices of order two by the Jacobi rotations computed similarly to [12]. This way the one-sided Jacobi SVD (and, similarly, the hyperbolic SVD) of real $n \times n$ matrices can be significantly sped up when n is small enough to make the eigendecompositions' execution time comparable to the 2×2 Grammian formations and the column updates, e.g., when the targeted matrices are the block pivots formed in a block-Jacobi algorithm [13, 14].

In numerical linear algebra the term “batched computation” is well-established, signifying a simultaneous processing of a large quantity of relatively small problems, e.g., the LU and the Cholesky factorizations [15] and the corresponding linear system solving [16] on the GPUs, with appropriate data layouts. It is therefore both justifiable and convenient to reuse the term in the present context.

This paper is organized as follows. A non-vectorized Kogbetliantz method for the SVD of a matrix of order two is presented in section 2. In section 3 a vector-friendly data layout is proposed, followed by a summary of the vectorized algorithm for the batched 2×2 SVDs in section 4. The algorithm comprises the following phases:

1. scaling the input matrices \mathbf{A} , each by a suitable power of two, to avoid any overflows and most underflows, vectorized in section 5 and based on subsection 2.1,
 2. the URV factorizations [17], vectorized in section 6 and based on subsection 2.2, of the matrices from the previous phase, into the real, non-negative, upper-triangular middle factors \mathbf{R} and the unitary left and right factors,
 3. the singular value decompositions of the factors \mathbf{R} from the previous phase, vectorized in section 7 and based on subsection 2.3, yielding the scaled $\mathbf{\Sigma}$, and
 4. assembling of the left (\mathbf{U}) and the right (\mathbf{V}) singular vectors of the matrices \mathbf{A} .
- The numerical testing results follow in section 8, and the conclusions in section 9.

2. The Kogbetliantz algorithm for the SVD of order two

The pointwise, non-vectorized Kogbetliantz algorithm for the SVD of a matrix of order two has been an active subject of research [18–20], and has been implemented for real matrices in LAPACK’s [21] `xLASV2` (for the full SVD) and `xLAS2` (for the singular values only) routines, where $\mathbf{x} \in \{\mathbf{S}, \mathbf{D}\}$. Here a simplified version of the algorithm from [4, trigonometric case] is described, with an early reduction of a complex matrix to the real one that is partly influenced by, but improves on, [22].

It is assumed in the paper that the floating-point arithmetic [23] is nonstop, i.e., does not trap on exceptions, and has the gradual underflow, i.e., Flush-denormals-To-Zero (FTZ) and Denormals-Are-Zero (DAZ) processor flags [6] are disabled.

To compute $|z|$ and $e^{i \arg z}$ for a complex z with both components finite, including $z = 0$, while avoiding the complex arithmetic operations, use the $\text{hypot}(a, b) = \sqrt{a^2 + b^2}$ function [5]. With `DBL_TRUE_MIN` being the smallest positive non-zero (and thus subnormal, or denormal in the old parlance) double precision value, let

$$\begin{aligned} |z| &= \text{hypot}(\Re z, \Im z), \quad e^{i \arg z} = \cos(\arg z) + i \cdot \sin(\arg z), \\ \cos(\arg z) &= \text{fmin}\left(\frac{|\Re z|}{|z|}, 1\right) \cdot \text{sign } \Re z, \quad \sin(\arg z) = \frac{\Im z}{\max(|z|, \text{DBL_TRUE_MIN})}. \end{aligned} \quad (1)$$

Here and in the following, `fmin` and `fmax` are the functions similar to the ones in the C language [5], but with a bit relaxed semantics, that return the minimal (respectively, maximal) of their two non-`NaN` arguments, or the second argument if the first is a `NaN`, as it is the case with the vector minimum and maximum [6, `VMINPD` and `VMAXPD`]. See also [7, subsection 6.2] for a similar exploitation of the `NaN` handling

of min and max operations. It now follows that, when $|z| = 0$, and so $\Re z = \Im z = 0$,

$$\cos(\arg z) = \text{sign } \Re z = \pm 1, \quad \sin(\arg z) = 0 \cdot \text{sign } \Im z = \pm 0.$$

The signs of $\Re z$ and $\Im z$ are thus preserved in $\cos(\arg z)$ and $\sin(\arg z)$, respectively.

A mandatory property of `hypot` for (1) to be applicable to all inputs z , where $\Re z$ and $\Im z$ are of sufficiently small magnitude (see subsection 2.1), is to have

$$\text{hypot}(a, b) = 0 \iff a = b = 0.$$

A vectorized `hypot` implementation is accessible from the Intel Short Vector Math Library (SVML) via a compiler intrinsic, as well as it is a reciprocal square root (`invsqrt` $x = 1/\sqrt{x}$) vectorized routine, helpful for the cosine calculations in (7), (15), and (16), though neither is always correctly rounded to at most half ulp^a.

2.1. *Exact scalings of the input matrix*

Even if both components of z are finite, $|z|$ from (1) can overflow, but $|2^{-1}z|$ cannot. Scaling a floating-point number by an integer power of two is exact, except when the significand of a subnormal result loses a trailing non-zero part due to shifting of the original significand to the left, or when the result overflows. Therefore, such scaling [6, `VSCALEFPD`] is the best remedy for the absolute value overflow problem.

Let the exponent of a floating-point value (assuming the radix two) be defined as $\exp_2 0 = -\infty$ and $\exp_2 a = \lfloor \lg |a| \rfloor$ for a finite non-zero a (see [6, `VGETEXPPD`]). Let $h = \text{DBL_MAX_EXP} - 3$ be two less than the largest exponent of a finite double precision number. To find a scaling factor 2^s for A , take s as

$$s = \min\{\text{DBL_MAX}, \min E^{\Re}, \min E^{\Im}\}, \quad (2)$$

where $E^{\Re} = \{E_{ij}^{\Re} \mid 1 \leq i, j \leq 2\}$ and $E^{\Im} = \{E_{ij}^{\Im} \mid 1 \leq i, j \leq 2\}$ are computed as

$$E_{ij}^{\Re} = h - \exp_2 \Re a_{ij}, \quad E_{ij}^{\Im} = h - \exp_2 \Im a_{ij}.$$

Note that $-2 \leq s \leq \text{DBL_MAX}$, due to the definition of h . If A is real, E^{\Im} is not used. The upper bound on s is required to be finite, since $0 \cdot 2^\infty$ would result in a NaN.

If there is a value of a huge magnitude (i.e., with its exponent greater than h) in A , s from (2) will be negative and the huge values will decrease, either twofold or fourfold. Else, s will be the maximal non-negative amount by which the exponents of the values in A can jointly be increased, thus taking the very small values out of the subnormal range if possible, without any of the new exponents going over h .

Let $\hat{A} = 2^s A$, and let \hat{a}_j denote the j th column of \hat{A} . The Frobenius norm of \hat{a}_j ,

$$\|\hat{a}_j\|_F = \text{hypot}(|\hat{a}_{1j}|, |\hat{a}_{2j}|). \quad (3)$$

cannot overflow (see (27) in the proof of Theorem 1 in subsection 2.3).

^aConsult the reports on the High Accuracy functions at <https://software.intel.com/content/www/us/en/develop/documentation/mkl-vmperfddata/top/real-functions/root.html> URL.

This scaling is both a simplification and an improvement of [4, subsection 2.3.2], which guarantees that the computed scaled singular values are finite, while avoiding any branching, lane masking, or recomputing when vectorized, with the only adverse effect being a potential sacrifice of the tiniest subnormal values in the presence of a huge one (i.e., with its exponent strictly greater than h) in A .

2.2. The URV factorization of a well-scaled matrix

If $\|\hat{a}_1\|_F < \|\hat{a}_2\|_F$, let $P_c = \begin{bmatrix} 0 & 1 \\ 1 & 0 \end{bmatrix}$, else let $P_c = \begin{bmatrix} 1 & 0 \\ 0 & 1 \end{bmatrix}$. Denote the column-pivoted \hat{A} by $A' = \hat{A}P_c$. If $|a'_{11}| < |a'_{21}|$, let $P_r^* = \begin{bmatrix} 0 & 1 \\ 1 & 0 \end{bmatrix}$, else let $P_r^* = \begin{bmatrix} 1 & 0 \\ 0 & 1 \end{bmatrix}$. Denote the row-sorted A' by $A'' = P_r^* A'$. To make a''_1 real and non-negative, let

$$D^* = \begin{bmatrix} e^{-i \arg a''_{11}} & 0 \\ 0 & e^{-i \arg a''_{21}} \end{bmatrix}, \quad A''' = D^* A''. \quad (4)$$

Complex multiplication, required in (4), (8), (9), and (11), is performed using the fused multiply-add operations with a single rounding [5], $\text{fma}(a, b, c) = a \cdot b + c$, as in [24, `cuComplex.h`] and [25, subsection 3.2.1], i.e., for a complex $c = a \cdot b$ holds

$$\Re c = \text{fma}(\Re a, \Re b, -\Im a \cdot \Im b), \quad \Im c = \text{fma}(\Re a, \Im b, \Im a \cdot \Re b). \quad (5)$$

To annihilate a'''_1 , compute the Givens rotation Q_α^* , where $-\pi/4 \leq \alpha \leq 0$, as

$$Q_\alpha^* = \cos \alpha \begin{bmatrix} 1 & -\tan \alpha \\ \tan \alpha & 1 \end{bmatrix}, \quad R'' = Q_\alpha^* \begin{bmatrix} a'''_1 & a'''_2 \end{bmatrix} = \begin{bmatrix} r_{11} & r'_{12} \\ 0 & r'_{22} \end{bmatrix}, \quad r_{11} = \|a'''_1\|_F. \quad (6)$$

Since the column norms of a well-scaled \hat{A} are finite, its column-pivoted, row-sorted QR factorization in (6) cannot result in an infinite element in R'' .

If $a'''_1 = 0$ then $A''' = 0$ as a special case. Handling special cases in a vectorized way is difficult as it implies branching or using the instructions with a lane mask. However, `fmax` function aids in avoiding both of these approaches similarly to `fmin` in (1), since $\tan \alpha$ and $\cos \alpha$ from (6) can be computed as

$$\tan \alpha = -\text{fmax}(a'''_{21}/a'''_{11}, 0), \quad \cos \alpha = \text{invsqrt}(\text{fma}(\tan \alpha, \tan \alpha, 1)). \quad (7)$$

To make r'_{12} from (5) real (see [22]) and non-negative, take \tilde{D} and obtain R' as

$$\tilde{D} = \begin{bmatrix} 1 & 0 \\ 0 & e^{-i \arg r'_{12}} \end{bmatrix}, \quad R' = R'' \tilde{D} = \begin{bmatrix} r_{11} & r_{12} \\ 0 & r'_{22} \end{bmatrix}, \quad r_{12} \geq 0. \quad (8)$$

Similarly, to make r'_{22} from (8) real and non-negative, take \hat{D}^* and obtain R as

$$\hat{D}^* = \begin{bmatrix} 1 & 0 \\ 0 & e^{-i \arg r'_{22}} \end{bmatrix}, \quad R = \hat{D}^* R' = \begin{bmatrix} r_{11} & r_{12} \\ 0 & r_{22} \end{bmatrix}, \quad r_{11} \geq \max\{r_{12}, r_{22}\}, \quad (9)$$

due to the column pivoting. Specifically, if A is already real, then

$$D^* = \begin{bmatrix} \text{sign } a''_{11} & 0 \\ 0 & \text{sign } a''_{21} \end{bmatrix}, \quad \tilde{D} = \begin{bmatrix} 1 & 0 \\ 0 & \text{sign } r'_{12} \end{bmatrix}, \quad \hat{D}^* = \begin{bmatrix} 1 & 0 \\ 0 & \text{sign } r'_{22} \end{bmatrix}. \quad (10)$$

6 *V. Novaković*

Note that, from (4), (6), (8), and (9),

$$R = U_+^* \hat{A} V_+, \quad U_+^* = \hat{D}^* Q_\alpha^* D^* P_r^*, \quad V_+ = P_c \tilde{D}, \quad (11)$$

where U_+^* and V_+ are unitary, i.e., $U_+ R V_+^*$ is a specific URV factorization [17] of \hat{A} .

2.3. The SVD of a special upper-triangular non-negative matrix

Here the plane rotations U_φ^* and V_ψ are computed, such that $U_\varphi^* R V_\psi = \Sigma'$, where

$$U_\varphi^* = \cos \varphi \begin{bmatrix} 1 & -\tan \varphi \\ \tan \varphi & 1 \end{bmatrix}, \quad V_\psi = \cos \psi \begin{bmatrix} 1 & \tan \psi \\ -\tan \psi & 1 \end{bmatrix}, \quad \Sigma' = \begin{bmatrix} \sigma'_{11} & 0 \\ 0 & \sigma'_{22} \end{bmatrix}, \quad (12)$$

with R from (9) and $\min\{\sigma'_{11}, \sigma'_{22}\} \geq 0$.

Let, as in [4, subsection 2.2.1], where the following formulas have been derived,

$$x = \text{fmax}(r_{12}/r_{11}, 0), \quad y = \text{fmax}(r_{22}/r_{11}, 0). \quad (13)$$

With x and y from (13), $0 \leq x, y \leq 1$, compute

$$\tan(2\varphi) = -\min \left\{ \text{fmax} \left(\frac{(2 \min(x, y)) \max(x, y)}{\text{fma}(x - y, x + y, 1)}, 0 \right), \sqrt{\text{DBL_MAX}} \right\}, \quad (14)$$

as justified in the next paragraph.

Since the quotient in (14) is non-negative (when defined), $\tan(2\varphi)$ is non-positive, and thus $-\pi/4 \leq \varphi \leq 0$. From $\tan(2\varphi)$ compute

$$\tan \varphi = \frac{\tan(2\varphi)}{1 + \sqrt{\text{fma}(\tan(2\varphi), \tan(2\varphi), 1)}}, \quad \cos \varphi = \text{invsqrt}(\sec^2 \varphi), \quad (15)$$

with $-1 \leq \tan \varphi \leq 0$ and $\sec^2 \varphi = \text{fma}(\tan \varphi, \tan \varphi, 1)$. Assume that $\tan(2\varphi)$ was not bounded in magnitude. If $|\tan(2\varphi)| = \infty$ in floating-point (this occurs rarely, when $x > 0$, $y = 1$, and $x \pm y = \pm 1$), then $\tan \varphi = \text{NaN}$ instead of the correct result, -1 . Else, if $|\tan(2\varphi)| > \sqrt{\text{DBL_MAX}}$, adding one to its square would have made little difference before the rounding (and the sum would have overflowed after it), so the square root in (15) could be approximated by $|\tan(2\varphi)|$. Again, with $|\tan(2\varphi)|$ so obtained, adding one to it in the denominator in (15) would have been irrelevant, and $\tan \varphi$ would have then equaled to -1 . Bounding $|\tan(2\varphi)|$ from above as in (14) therefore avoids the argument of the square root overflowing (so using $\text{hypot}(\tan(2\varphi), 1)$ instead of $\sqrt{\text{fma}(\tan(2\varphi), \tan(2\varphi), 1)}$ is not required), and ensures $\tan \varphi = -1$ for all $\tan(2\varphi)$ that would otherwise be greater than the bound.

Having thus computed U_φ , the right plane rotation V_ψ is constructed from

$$\tan \psi = \text{fma}(y, \tan \varphi, -x), \quad \cos \psi = \text{invsqrt}(\sec^2 \psi), \quad (16)$$

where $\tan \psi \leq 0$ and $\sec^2 \psi = \text{fma}(\tan \psi, \tan \psi, 1)$.

The following Theorem 1 shows that the special form of R contributes to an important property of the computed scaled singular values Σ' ; namely, they are already sorted non-ascendingly, and thus never have to be swapped in a postprocessing step. Also, the scaled singular values are always finite in floating-point arithmetic.

Theorem 1. For Σ' it holds $\infty > \sigma'_{11} \geq \sigma'_{22} \geq 0$, where

$$\sigma'_{11} = (\cos \varphi \cos \psi \sec^2 \psi) r_{11}, \quad \sigma'_{22} = (\cos \varphi \cos \psi \sec^2 \varphi) r_{22}, \quad (17)$$

and $\sqrt{2} \geq |\tan \psi| \geq |\tan \varphi| \geq 0$.

Proof. Assume $r_{12} > 0$ in (9), i.e., $x > 0$ in (13). Else, from (13), (14), and (16), both tangents are zero and both cosines are unity, thus from (12) and (9) follows $\sigma'_{11} = r_{11} \geq r_{22} = \sigma'_{22}$, as claimed, and only $\sigma'_{11} < \infty$ remains to be proven.

From (15) $\cos \varphi \neq 0$, and from (16) $\tan \psi \neq -\infty$, so $\cos \psi \neq 0$. Scaling U_φ^* by $1/\cos \varphi$ and V_ψ by $1/\cos \psi$ in (12), and R by $1/r_{11}$ in (9), from (13) follows

$$\begin{bmatrix} 1 & -\tan \varphi \\ \tan \varphi & 1 \end{bmatrix} \begin{bmatrix} 1 & x \\ 0 & y \end{bmatrix} \begin{bmatrix} 1 & \tan \psi \\ -\tan \psi & 1 \end{bmatrix} = \begin{bmatrix} \sigma''_{11} & 0 \\ 0 & \sigma''_{22} \end{bmatrix}. \quad (18)$$

Multiplying the matrices on the left hand side of (18) and equating the elements of the result with the corresponding elements of the right hand side, one obtains

$$\sigma''_{11} = \tan^2 \psi + 1 = \sec^2 \psi, \quad \sigma''_{22} = (\tan^2 \varphi + 1)y = (\sec^2 \varphi)y, \quad (19)$$

after an algebraic simplification using the relation (16) for $\tan \psi = y \tan \varphi - x$. The equations for σ'_{11} and σ'_{22} from (17) then follow by multiplying the equations for σ''_{11} and σ''_{22} from (19), respectively, by $r_{11} \cos \varphi \cos \psi$. Specially, $\sigma'_{11} > 0$, since $\sigma'_{11} = 0$ would imply an obvious contradiction $r_{11} = 0 \geq r_{12} > 0$ with the assumption.

If $y = 0$, from (19) and (17) it follows $\sigma'_{11} > 0 = \sigma'_{22} = \sigma'_{22}$, and, due to (14), (15), and (16), it holds $|\tan \psi| = x > 0 = |\tan \varphi|$. If $y = 1$ then $x = 0$ from (9) and (13), contrary to the assumption. Therefore, $0 < y < 1$ in the following, and let

$$a = -2xy < 0, \quad b = 1 + x^2 - y^2 > 0, \quad c = b + \sqrt{a^2 + b^2} > 0. \quad (20)$$

Then, rewrite $\tan(2\varphi)$ from (14) using (20) as

$$\tan(2\varphi) = \frac{a}{b}, \quad \tan^2(2\varphi) + 1 = \frac{a^2 + b^2}{b^2}, \quad (21)$$

as well as $\tan \varphi$ from (15) using (21) and (20) as

$$\tan \varphi = \frac{\tan(2\varphi)}{1 + \sqrt{\tan^2(2\varphi) + 1}} = \frac{a/b}{(b + \sqrt{a^2 + b^2})/b} = \frac{a}{b + \sqrt{a^2 + b^2}} = \frac{a}{c}. \quad (22)$$

From (22), $|\tan \varphi| = |a|/c > 0$, what gives $|\tan \psi| = y|a|/c + x$ with (13) and (16). Taking the ratio of these two absolute values, it has to be proven that

$$\frac{|\tan \psi|}{|\tan \varphi|} = \frac{|a|y + cx}{|a|} \geq 1. \quad (23)$$

Expanding (23) using (20), it follows

$$\frac{|a|y}{|a|} + \frac{cx}{|a|} = y + \frac{(1 + x^2 - y^2 + \sqrt{a^2 + b^2})x}{2xy} = \frac{1 + x^2 + y^2 + \sqrt{a^2 + b^2}}{2y}, \quad (24)$$

where the argument of the square root can be expressed as

$$a^2 + b^2 = (1 + x^2)^2 + 2(x^2 - 1)y^2 + y^4, \quad (25)$$

8 *V. Novaković*

after substitution of (20) for a and b and a subsequent algebraic simplification. For a fixed but arbitrary y , (25), and thus the numerator of (24), decrease monotonically as $x \rightarrow 0$. Substituting zero for x in (24) and (25), the former becomes

$$\frac{1 + y^2 + \sqrt{(1 - y^2)^2}}{2y} = \frac{2}{2y} = \frac{1}{y} > 1,$$

what proves the inequality between the tangents.

The inequality between the scaled singular values follows easily from (19) as

$$\frac{\sigma'_{22}}{\sigma'_{11}} = \frac{\sigma''_{22}}{\sigma''_{11}} = \frac{\tan^2 \varphi + 1}{\tan^2 \psi + 1} y < 1,$$

since $\tan^2 \psi \geq \tan^2 \varphi$ and $y < 1$. It remains to be shown that $\sigma'_{11} < \infty$ for all R from (9). If R has not been computed (what is never the case in the proposed method) from a well-scaled \hat{A} (see subsection 2.1), then even σ'_{22} can overflow.

Observe that $1/\sqrt{2} < \cos \varphi \leq 1$ from (14), and $0 < \cos \psi \leq \cos \varphi$. From (17),

$$\frac{\sigma'_{11}}{r_{11}} = \frac{\cos \varphi}{\cos \psi} \leq \frac{1}{\cos \psi}. \quad (26)$$

Since, from (15) and (16),

$$|\tan \psi| = y|\tan \varphi| + x \leq y + x, \quad \cos \psi = 1/\sqrt{1 + \tan^2 \psi},$$

$x + y$ has to be bounded from above, to be able to bound $\cos \psi$ from below, and thus (26) from above. From (9) and the column pivoting goal, $r_{11}^2 \geq r_{12}^2 + r_{22}^2$, what gives $x^2 + y^2 \leq 1$ after dividing by r_{11}^2 , i.e., x and y are contained in the intersection of the first quadrant and the unit disc. On this domain, $x + y$ attains the maximal value of $\sqrt{2}$ for $x = y = 1/\sqrt{2}$, so $|\tan \psi| \leq \sqrt{2}$, as claimed, and thus $\cos \psi \geq 1/\sqrt{3}$. Substituting this lower bound for $\cos \psi$ in (26), it follows $\sigma'_{11} \leq \sqrt{3} \cdot r_{11} \ll 2 \cdot r_{11}$.

From subsection 2.1 and (6), since

$$\max_{1 \leq i, j \leq 2} \{|\Re \hat{a}_{ij}|, |\Im \hat{a}_{ij}|\} < 2^{h+1},$$

it can be concluded that

$$\max_{1 \leq i, j \leq 2} |\hat{a}_{ij}| < \sqrt{(2^{h+1})^2 + (2^{h+1})^2} = \sqrt{2} \cdot 2^{h+1},$$

and therefore

$$r_{11} = \max_{1 \leq j \leq 2} \|\hat{a}_j\|_F < \sqrt{(\sqrt{2} \cdot 2^{h+1})^2 + (\sqrt{2} \cdot 2^{h+1})^2} = 2 \cdot 2^{h+1} = 2^{h+2}, \quad (27)$$

so $\sigma'_{11} \ll 2 \cdot 2^{h+2} = 2^{h+3}$, where the right hand side is the immediate successor (that represents ∞) of the largest finite floating-point number, as claimed. \square

Using Theorem 1, from (12) and (11) then follows

$$\Sigma = 2^{-s} \Sigma', \quad U^* = U_\varphi^* U_+^*, \quad V = V_+ V_\psi, \quad U = (U^*)^*, \quad (28)$$

where Σ' has to be backscaled to obtain the singular values of the original input matrix. However, the backscaling should be skipped if it would cause the singular values to overflow or (less catastrophic but still inaccurate outcome) underflow, while informing the user of such an event by preserving the value of s .

Specifically, by matrix multiplication, from (28) and (11) it follows

$$\begin{aligned} U &= \cos \alpha \cos \varphi P_r \begin{bmatrix} d_{11}(1 - \hat{d}_{22} \tan \alpha \tan \varphi) & d_{11}(\tan \varphi + \hat{d}_{22} \tan \alpha) \\ -d_{22}(\tan \alpha + \hat{d}_{22} \tan \varphi) & d_{22}(\hat{d}_{22} - \tan \alpha \tan \varphi) \end{bmatrix}, \\ V &= \cos \psi P_c \begin{bmatrix} 1 & \tan \psi \\ -\tilde{d}_{22} \tan \psi & \tilde{d}_{22} \end{bmatrix}. \end{aligned} \quad (29)$$

Computing each element of a complex U requires only one complex multiplication.

Writing a complex number z as $(\Re z, \Im z) = \Re z + i \cdot \Im z$, noting that d_{11} , d_{22} , and \hat{d}_{22} are the complex conjugates of $(D^*)_{11}$, $(D^*)_{22}$, and $(\hat{D}^*)_{22}$, respectively, and precomputing $c = \cos \alpha \cos \varphi$ and $t = -\tan \alpha \tan \varphi$, (29) can be expanded as, e.g.,

$$\begin{aligned} (P_r^* U)_{11} &= c(d_{11} \cdot (\text{fma}(\Re \hat{d}_{22}, t, 1), \Im \hat{d}_{22} t)), \\ (P_r^* U)_{21} &= -c(d_{22} \cdot (\text{fma}(\Re \hat{d}_{22}, \tan \varphi, \tan \alpha), \Im \hat{d}_{22} \tan \varphi)), \\ (P_r^* U)_{12} &= c(d_{11} \cdot (\text{fma}(\Re \hat{d}_{22}, \tan \alpha, \tan \varphi), \Im \hat{d}_{22} \tan \alpha)), \\ (P_r^* U)_{22} &= c(d_{22} \cdot (\text{fma}(-\tan \alpha, \tan \varphi, \Re \hat{d}_{22}), \Im \hat{d}_{22})), \end{aligned}$$

but another mathematically equivalent computation that minimizes the number of roundings required for forming the elements of $P_r^* U$ as this one does is also valid.

3. Vector-friendly data layout

Vectors replace scalars in the SIMD arithmetic operations. A vector should hold S elements from the same matrix sequence, with the same row and column indices, and the consecutive bracketed indices. When computing with complex numbers, however, it is more efficient to keep the real and the imaginary parts of the elements in separate vectors, since there are no hardware vector instructions for the complex multiplication and division, e.g., which thus have to be implemented manually. Also, a vector should be aligned in memory to a multiple of W bytes to employ the most efficient versions of the vector load/store operations. It is therefore essential to establish a vector-friendly layout for the matrix sequences \mathbf{A} , \mathbf{U} , \mathbf{V} , and Σ' in the linear memory space. One such layout, inspired by splitting the real and the complex parts of the matrix elements into separate vectors [7, subsection 6.2], is

$$\Re \mathbf{a}_{ij} = \boxed{\Re a_{ij}^{[1]}} \boxed{\Re a_{ij}^{[2]}} \cdots \boxed{\Re a_{ij}^{[\hat{n}]}} \quad, \quad \Im \mathbf{a}_{ij} = \boxed{\Im a_{ij}^{[1]}} \boxed{\Im a_{ij}^{[2]}} \cdots \boxed{\Im a_{ij}^{[\hat{n}]}}.$$

where $\Re \mathbf{a}_{ij}$ and $\Im \mathbf{a}_{ij}$ (similarly, $\Re \mathbf{u}_{ij}$, $\Im \mathbf{u}_{ij}$, and $\Re \mathbf{v}_{ij}$, $\Im \mathbf{v}_{ij}$) for $i, j \in \{1, 2\}$ are the sequences of the real and the imaginary components, respectively, of the elements in the i th row and the j th column of the matrices in \mathbf{A} (similarly, in \mathbf{U} and in \mathbf{V}).

Each train of boxes represents a contiguous region of memory aligned to W bytes. In the real case, no \mathfrak{S} -boxes exist, but the layout otherwise stays the same. The scaled singular values $\sigma'_{\max}^{[k]}$ and $\sigma'_{\min}^{[k]}$ from (12) are stored as

$$\boldsymbol{\sigma}'_{\max} = \boxed{\sigma'_{\max}^{[1]}} \boxed{\sigma'_{\max}^{[2]}} \cdots \boxed{\sigma'_{\max}^{[\hat{n}]}} , \quad \boldsymbol{\sigma}'_{\min} = \boxed{\sigma'_{\min}^{[1]}} \boxed{\sigma'_{\min}^{[2]}} \cdots \boxed{\sigma'_{\min}^{[\hat{n}]}} ,$$

respectively, while the scaling parameters $s^{[k]}$ from (2) are laid out as

$$\mathbf{s} = \boxed{s^{[1]}} \boxed{s^{[2]}} \cdots \boxed{s^{[\hat{n}]}} .$$

The virtual elements, with their bracketed indices ranging from $n+1$ to \hat{n} , serve if present as a (e.g., zero) padding, which ensures that all vectors, including the last one, formed from the consecutive elements of a box train, hold the same maximal number (S) of defined values and can thus be processed in an uniform manner.

The input sequence \mathbf{A} may initially be in another layout and has to be repacked before any further computation. Also, the output sequences \mathbf{U} , \mathbf{V} , $\boldsymbol{\Sigma}'$, and \mathbf{s} may have to be repacked for a further processing. Such reshufflings should be avoided, as they incur a substantial overhead in both time and memory requirements.

Layout of data, including the intermediate results, in vector registers during the computation is the same as it is for the box trains, but with S elements instead of \hat{n} . The v th vector, for $1 \leq v \leq V = \hat{n}/S$, encompasses the consecutive indices k ,

$$(v-1) \cdot S + 1 \leq k \leq v \cdot S. \quad (30)$$

A vector is loaded into, kept in, and stored from, a variable of the C type `_mm512d`.

In the following, a bold lowercase letter stands for a vector, and the uppercase one for a (logical, not necessarily in-memory) matrix sequence. For example, \mathbf{R} is a sequence of \hat{n} matrices $R^{[k]}$, of which $\mathbf{R}[v]$ is a subsequence of length S , and $\mathbf{r}_{12}[v]$ is a vector containing elements $r_{12}^{[k]}$ of $\mathbf{R}^{[k]}$, for some v and its corresponding indices k from (30). A bold constant denotes a vector with all its values being equal to the given constant. An arithmetic operation on vectors (or collections thereof) or matrix sequences is a shorthand for a sequence of the elementwise operations; e.g.,

$$\mathbf{2}^{-\mathbf{s}} = (2^{-s^{[k]}})_k, \quad \mathbf{BC} = (B^{[k]}C^{[k]})_k, \quad 1 \leq k \leq \hat{n}.$$

where \mathbf{B} and \mathbf{C} are any two matrix sequences, $B^{[k]}C^{[k]}$ is a product of matrices of order two, and $\mathbf{2}$ is a collection of vectors with all their values equal to two. All bracketed indices are one-based, as it is customary in linear algebra, but in the C code they are zero-based, being thus one less than they are in the paper's text.

4. Overview of the algorithm for the batched SVDs of order two

When there are two cases, the real and the complex one, all code-presenting figures cover the latter with a mixture of the actual statements and a mathematically oriented pseudocode. The real-case differences are described in them in the comments starting with \mathbb{R} . A function name in uppercase, `NAME`, is a shorthand for the `_mm512_name_pd` C compiler intrinsic, if the operation is available in the machine's

$$\begin{aligned} \text{NAME}(x, y) &= \text{_mm512_castsi512_pd}(\text{_mm512_name_epi64}(\hat{x}, \hat{y})), \\ \hat{x} &= \text{_mm512_castpd_si512}(x), \quad \hat{y} = \text{_mm512_castpd_si512}(y). \end{aligned}$$

The four phases of the algorithm for the batched SVDs of order two, as listed in section 1, can be succinctly depicted by the following logical execution pipeline,

where the first row shows the transformations of \mathbf{A} , the second row contains the various matrix sequences that are the “by-products” of the computation, described in section 2, ending with the sequences of the left and the right singular vectors, that are formed as indicated in the third row. As the singular values Σ can overflow due to the backscaling (see subsection 2.3) of the scaled ones (Σ'), computing them unconditionally is unsafe, and such postprocessing is left to the user’s discretion. In certain use-cases it might be known in advance that the singular values cannot overflow/underflow, e.g., if the initial matrices have already been well-scaled at their formation. The backscaling, performed as in Fig. 1, is then unconditionally safe.

```

1  -0 = SET1(-0.0); // a constant vector with all lanes equal to -0.0
2  -s[v] = XOR(s[v], -0); // negation is performed as XOR-ing with -0
3   $\sigma_{\max}[v] = \text{SCALEF}(\sigma'_{\max}[v], -s[v]); \sigma_{\min}[v] = \text{SCALEF}(\sigma'_{\min}[v], -s[v]);$ 
4  s[v] = -0; // inform the user that the backscaling has been performed

```

Fig. 1. Optional vectorized backscaling of Σ' to Σ by 2^{-s} .

The pipeline is executed independently on each non-overlapping subsequence of S consecutive matrices. If there are more such sequences than the active threads, at a point in time some sequences might have already been processed, while the others are still waiting, either for the start or the completion of the processing. A conceptual core of a driver routine implementing such a pass over the data is shown in Fig. 2, where $\mathbf{xSsvd2}$, $\mathbf{x} \in \{\mathbf{d}, \mathbf{z}\}$, are the main (real or complex, respectively), single-threaded routines that are responsible for all vectorized computations on each

particular sequence of size S . The OpenMP [26] `parallel for` directive in Fig. 2 assumes a user-defined maximal number and placement/affinity of threads.

```

1  const size_t V = (n + (S - 1)) / S; // V =  $\lceil n/S \rceil$ ,  $\hat{n} = V \cdot S$ 
2  #pragma omp parallel for shared(V, A, U, V,  $\Sigma'$ , s)
3  for (size_t v = 0; v < V; ++v) xSsvd2(A[v], U[v], V[v],  $\Sigma'[v]$ , s[v]);

```

Fig. 2. A conceptualization of the main part of a driver routine for the batched SVDs of order two, with an OpenMP parallel loop over the data, where each of the V subsequences of length S can be processed concurrently with others by an `xSsvd2` routine that performs S SVDs simultaneously.

The input arguments of `xSsvd2` are (the pointers to) the arrays, each aligned to W bytes, of S `double` values, e.g., `const double A12r[static S]` for $\Re \mathbf{a}_{12}[v]$. The output arguments are similar, e.g., `double U21i[static S]` for $\Im \mathbf{u}_{21}[v]$. Note that the same interface, up to replacing S by 1, would be applicable to the pointwise `x1svd2` routine for a single 2×2 SVD, but without the implied alignment restriction.

No branching is involved explicitly in the `xSsvd2` routines. It is therefore fully branch-free, if the used SVML routines are. All data, once loaded from memory or computed, is intended to be held in the `zmm` vector registers until the output has been formed and written back to RAM. This goal is almost achievable in the test setting, since there are two vector register spillages, with a total of only four extra memory accesses (two writes and two reads), as reported by the optimizer. A hand-tuned self-contained assembly might do away with these as well.

The first three phases of the algorithm are vectorized as described in sections 5, 6, and 7, respectively, since each of the phases can be viewed as an algorithm on its own. They are, however, chained by the dataflow, each having as its input the output of the previous one. Should the output of a phase be made available alongside the final results, it could be written to an additional memory buffer in the same layout as presented in section 3. Otherwise, the intermediate results are not preserved.

Vectorization of the last, fourth phase of the algorithm from (29) is as tedious and uninformative as it is straightforward, and so it is omitted for brevity. It suffices to say that $\Re \mathbf{u}_{ij}$ (and $\Im \mathbf{u}_{ij}$) and $\Re \mathbf{v}_{ij}$ (and $\Im \mathbf{v}_{ij}$), for $1 \leq i, j \leq 2$, are computed from (29), using the `fma` operation where possible, and (5) for the complex multiplications. The final row permutations by \mathbf{P}_r or \mathbf{P}_c are performed in the same way as the row swaps in the URV factorization phase, described in Fig. 6 in section 6. An interested reader is referred to the actual code in the supplementary material^b.

5. Vectorized exact scalings of the input matrices

Computation of the scaling parameters \mathbf{s} is remarkably simple, as shown in Fig. 3. It is advantageous to have `GETEXP(a) = exp2(a)` and `SCALEF(a, b) = a · 2b` vector

^bSupplementary material is available in <https://github.com/venovako/VecKog> repository.

```

1 h = SET1((double)(DBL_MAX_EXP-3)); // set each lane of h to h
2  $\mathbf{e}_{ij}^{\mathcal{R}}[\mathbf{v}]$  = SUB(h, GETEXP( $\mathcal{R}\mathbf{a}_{ij}[\mathbf{v}]$ )); //  $\mathbf{h} - \exp_2 \mathcal{R}\mathbf{a}_{ij}[\mathbf{v}]$ 
3 // take  $\mathbf{e}^{\mathcal{R}}[\mathbf{v}] = \min\{\mathbf{e}_{11}^{\mathcal{R}}[\mathbf{v}], \mathbf{e}_{21}^{\mathcal{R}}[\mathbf{v}], \mathbf{e}_{12}^{\mathcal{R}}[\mathbf{v}], \mathbf{e}_{22}^{\mathcal{R}}[\mathbf{v}]\}$  by a two-level min-reduction
4  $\mathbf{e}^{\mathcal{R}}[\mathbf{v}]$  = MIN(MIN( $\mathbf{e}_{11}^{\mathcal{R}}[\mathbf{v}], \mathbf{e}_{21}^{\mathcal{R}}[\mathbf{v}]$ ), MIN( $\mathbf{e}_{12}^{\mathcal{R}}[\mathbf{v}], \mathbf{e}_{22}^{\mathcal{R}}[\mathbf{v}]$ ));
5 //  $\mathbf{e}_{ij}^{\mathcal{S}}[\mathbf{v}]$ , with  $1 \leq i, j \leq 2$ , and  $\mathbf{e}^{\mathcal{S}}[\mathbf{v}]$  are computed analogously from  $\mathcal{S}\mathbf{a}_{ij}[\mathbf{v}]$ 
6 s[v] = MIN(SET1(DBL_MAX), MIN( $\mathbf{e}^{\mathcal{R}}[\mathbf{v}], \mathbf{e}^{\mathcal{S}}[\mathbf{v}]$ )); // from (2),  $\mathbb{R}$ :  $\mathbf{e}^{\mathcal{S}}[\mathbf{v}]$  nonexistent
7  $\mathcal{R}\hat{\mathbf{a}}_{ij}[\mathbf{v}]$  = SCALEF( $\mathcal{R}\mathbf{a}_{ij}[\mathbf{v}], \mathbf{s}[\mathbf{v}]$ );  $\mathcal{S}\hat{\mathbf{a}}_{ij}[\mathbf{v}]$  = SCALEF( $\mathcal{S}\mathbf{a}_{ij}[\mathbf{v}], \mathbf{s}[\mathbf{v}]$ );

```

Fig. 3. Vectorized computation of the scaling parameters **s** from (2) and the scaling of **A**.

operations, returning a correct (or correctly rounded, respectively) result, even with subnormal inputs (the former) or outputs (the latter). Should they not be available on another platform, their scalar variants (`frexp` and `scalbn`, respectively) might be used instead on the values in each lane, slowing the execution considerably.

Once $\hat{\mathbf{A}}$ is obtained from **A**, the column norms of the former are computed as in Fig. 4. Observe that $\text{ABS}(\mathbf{b}) = \text{ANDNOT}(-\mathbf{0}, \mathbf{b})$, since $\text{ANDNOT}(\mathbf{a}, \mathbf{b}) = \neg \mathbf{a} \wedge \mathbf{b}$ bitwise, and that having a vectorized `HYPOT` is essential here. Should it not be available, it would have to be carefully implemented to avoid the overflows in the intermediate results. A naïve per-lane computation of $c = \text{hypot}(a, b)$, where a and b are finite, without adjusting the exponents of a and b , but with one extra division instead, is to let $a' = \max\{|a|, |b|\}$, $b' = \min\{|a|, |b|\}$, $a^+ = \max\{a', \text{DBL_TRUE_MIN}\} > 0$, $q^+ = b'/a^+ \leq 1$, and $c = a' \cdot \sqrt{\text{fma}(q^+, q^+, 1)}$.

```

1  $|\hat{\mathbf{a}}_{ij}|[\mathbf{v}]$  = HYPOT( $\mathcal{R}\hat{\mathbf{a}}_{ij}[\mathbf{v}], \mathcal{S}\hat{\mathbf{a}}_{ij}[\mathbf{v}]$ ); // from (1),  $\mathbb{R}$ :  $|\hat{\mathbf{a}}_{ij}|[\mathbf{v}] = \text{ANDNOT}(-\mathbf{0}, \mathcal{R}\hat{\mathbf{a}}_{ij}[\mathbf{v}])$ 
2  $\|\hat{\mathbf{a}}_j\|_F[\mathbf{v}]$  = HYPOT( $|\hat{\mathbf{a}}_{1j}|[\mathbf{v}], |\hat{\mathbf{a}}_{2j}|[\mathbf{v}]$ ); // with  $j \in \{1, 2\}$ , from (3)

```

Fig. 4. Vectorized computation of the column norms $\|\hat{\mathbf{a}}_j\|_F$ from (3).

6. Vectorized URV factorizations of order two

Having its column norms computed, $\hat{\mathbf{A}}$ has to be pivoted, each matrix by a column-swapping permutation (or identity, if a swap is not required), such that a column with the largest norm becomes the first one. This is accomplished in Fig. 5 by the `MASK_BLEND` operation, that selects a value for the ℓ th output lane from the same lane in either the first or the second argument vector, according to a bit-mask **C** that compactly encodes the results of the lane-wise $<$ -comparisons of the norms by the `CMPLT_MASK` operation. If the ℓ th bit in the mask is zero (i.e., the ℓ th comparison is false), the ℓ th output lane gets its value from the first vector, and the corresponding permutation $\mathbf{P}_c^{[k]}$, where $k = (\mathbf{v} - 1) \cdot \mathbf{S} + \ell$, is identity; else, the output value is taken from the second vector, and the permutation encodes a swap. All norms are finite and thus ordered, so the complement of the relation $<$ is \geq .

```

1  c[v] = CMPLT_MASK(||â1||F[v], ||â2||F[v]); // S-bit mask encodes the < relation
2  ℑa'i1[v] = MASK_BLEND(c[v], ℑâi1[v], ℑâi2[v]); // similarly for ℑa'i1[v]
3  ℑa'i2[v] = MASK_BLEND(c[v], ℑâi2[v], ℑâi1[v]); // similarly for ℑa'i2[v]
4  |a'i1|[v] = MASK_BLEND(c[v], |âi1||[v], |âi2||[v]);
5  |a'i2|[v] = MASK_BLEND(c[v], |âi2||[v], |âi1||[v]);
6  ||a'1||F[v] = MASK_BLEND(c[v], ||â1||F[v], ||â2||F[v]);
7  ||a'2||F[v] = MASK_BLEND(c[v], ||â2||F[v], ||â1||F[v]);

```

Fig. 5. Vectorized column pivoting of $\hat{\mathbf{A}}$.

Not only \mathbf{A}' itself has to be obtained. The absolute values of the elements and the column norms also have to be subject to the same (maybe identity) permutations, as in Fig. 5, to avoid recomputing them unnecessarily and at a greater cost, especially in the complex case. The similar principles hold for the row sorting of \mathbf{A}' in Fig. 6.

```

1  r[v] = CMPLT_MASK(|a'11||[v], |a'21||[v]); // Is |a'11||[v] < |a'21||[v], lane-wise?
2  ℑa''1j[v] = MASK_BLEND(r[v], ℑa'1j[v], ℑa'2j[v]); // similarly for ℑa''1j[v]
3  ℑa''2j[v] = MASK_BLEND(r[v], ℑa'2j[v], ℑa'1j[v]); // similarly for ℑa''2j[v]
4  |a''1j|[v] = MASK_BLEND(r[v], |a'1j||[v], |a'2j||[v]);
5  |a''2j|[v] = MASK_BLEND(r[v], |a'2j||[v], |a'1j||[v]);

```

Fig. 6. Vectorized row sorting of \mathbf{A}' .

Since only the rows of \mathbf{A}' are possibly swapped to get \mathbf{A}'' , the column norms do not change, so $\|\mathbf{a}''_j\|_F = \|\mathbf{a}'_j\|_F$. To make the first columns of \mathbf{A}'' real and non-negative, \mathbf{D}^* from (4) or (10) is computed and applied as in Fig. 7. Observe how the sign extractions and the implicit complex conjugations and multiplications are performed in Fig. 7, as the same pattern is assumed for them in the following.

The matrices \mathbf{D}^* are unitary and diagonal, so $\|\mathbf{a}'''_j\|_F = \|\mathbf{a}''_j\|_F$ can be (and is) assumed, though numerically they might slightly differ, should the former be recomputed, due to the rounding errors accumulated in the course of the transformations of the elements of \mathbf{A}'' as in Fig. 7, as well as due to the recomputation itself.

Fig. 8 shows how to get the QR factorizations from (6), i.e., $\mathbf{R}'' = \mathbf{Q}_\alpha^* \mathbf{A}'''$. Only \mathbf{r}'_2 has to be computed by multiplying \mathbf{a}'''_2 (complex in the general case) from the left by the real \mathbf{Q}_α^* , while \mathbf{r}'_1 is always real and already known. Should `INVSQRT` not be available, there are two remedies, both starting from $\sec \alpha = \sqrt{1 + \tan^2 \alpha}$. The first, faster one computes $\cos \alpha = 1 / \sec \alpha$, while the second, possibly more accurate one due to requiring one rounding less than the first [4], does not require the cosine at all, and instead replaces all multiplications by it with divisions by the secant.

Now \mathbf{r}'_{12} has to be made real and non-negative by multiplying \mathbf{R}'' by $\tilde{\mathbf{D}}$ from the right, obtaining \mathbf{R}' as in (8), and then \mathbf{r}'_{22} has to undergo a similar procedure

```

1  1 = SET1(1.0); m = SET1(DBL_TRUE_MIN); // ones & the successors of +0
2  |ai1+[v] = MAX(|ai1''[v], m); // from (1), with i ∈ {1, 2}, here and below
3  Rdii[v] = OR(MIN(DIV(ANDNOT(-0, Rai1''[v]), |ai1''[v]), 1), AND(Rai1''[v], -0));
4  Sdii[v] = DIV(Sai1''[v], |ai1+[v]); // Sdii*[v] = -Sdii[v] implicitly
5  // R: Rdii[v] = AND(Rai1''[v], -0), only the sign bit (±0, not ±1 from (10))
6  // (Rai2''[v], Sai2''[v]) = (Rdii*[v], Sdii*[v]) · (Rai2''[v], Sai2''[v]), from (4)
7  Rai2'''[v] = FMADD(Rdii[v], Rai2''[v], MUL(Sdii[v], Sai2''[v])); // and below from (5)
8  Sai2'''[v] = FMSUB(Rdii[v], Sai2''[v], MUL(Sdii[v], Rai2''[v])); // Fused Mul and SUB
9  // R: Rai2'''[v] = XOR(Rdii[v], Rai2''[v]), Rai2'''[v] = Rdii*[v] · Rai2''[v] from (10)
10 Rai1'''[v] = |ai1''[v]; // assume Sai1''[v] = SETZERO(); i.e., 0

```

Fig. 7. Vectorized computation of \mathbf{D}^* and \mathbf{A}''' from (4) or (10).

```

1  r11[v] = ||a1'''||F[v]; // from (6), r21[v] = 0 is assumed but not set
2  -tan α[v] = MAX(DIV(Ra21'''[v], Ra11'''[v]), 0); // from (7)
3  cos α[v] = INVSQRT(FMADD(tan α[v], tan α[v], 1)); // from (7)
4  Rr12'[v] = MUL(cos α[v], FMADD(-tan α[v], Ra22'''[v], Ra12'''[v])); // similarly Sr12'[v]
5  // tan α[v] implicit in Fused_Negative_Multiply-ADD(a, b, c) = -(a · b) + c
6  Rr22''[v] = MUL(cos α[v], FNMADD(-tan α[v], Ra12'''[v], Ra22'''[v])); // Sr22''[v] likewise

```

Fig. 8. The vectorized QR factorization of \mathbf{A}''' from (6) and (7).

by multiplying \mathbf{R}' from the left by $\widehat{\mathbf{D}}^*$, as in (9), to get the real and non-negative \mathbf{R} . The first step involves one complex multiplication per lane, $\mathbf{r}'_{22} = \mathbf{r}''_{22} \cdot \tilde{\mathbf{d}}_{22}$, while $\mathbf{r}_{12} = |\mathbf{r}'_{12}|$, and the second step involves none, since $\mathbf{r}_{22} = |\mathbf{r}'_{22}|$, as shown in Fig. 9.

7. Vectorized SVD of real upper-triangular matrices of order two

In Fig. 10 a vectorization of the 2×2 SVD method from subsection 2.3 for non-negative upper triangular matrices is shown. If $\mathbf{T} \neq \text{double}$, the precomputed upper bound for $\tan(2\varphi)$ should be replaced by the appropriate one (e.g., for $\mathbf{T} = \text{float}$, $\sqrt{\text{FLT_MAX}}$ should be used instead). No sines are explicitly computed here, unlike in the LAPACK's DLASV2 routine, but could be, as $\sin \beta = \cos \beta \cdot \tan \beta$, for $\beta \in \{\varphi, \psi\}$.

A computation functionally similar to the one proposed in Fig. 10 could be performed by **S** calls to DLASV2. In the Fortran syntax, one such call looks like

```
CALL DLASV2(F[k], G[k], H[k], SSMIN[k], SSMAX[k], SNR[k], CSR[k], SNL[k], CSL[k]),
```

where k lies in the range (30), for a given \mathbf{v} . The input-only arguments are

$$\mathbf{F}^{[k]} = \mathbf{r}_{11}^{[k]}, \quad \mathbf{G}^{[k]} = \mathbf{r}_{12}^{[k]}, \quad \mathbf{H}^{[k]} = \mathbf{r}_{22}^{[k]},$$

```

1   $\mathbf{r}_{12}[\mathbf{v}] = |\mathbf{r}'_{12}[\mathbf{v}]| = \text{HYPOT}(\Re'_{12}[\mathbf{v}], \Im'_{12}[\mathbf{v}]); // \mathbb{R}: \mathbf{r}_{12}[\mathbf{v}] = \text{ANDNOT}(-\mathbf{0}, \Re'_{12}[\mathbf{v}])$ 
2   $\Re\hat{\mathbf{d}}_{22}^* = \text{OR}(\text{MIN}(\text{DIV}(\text{ANDNOT}(-\mathbf{0}, \Re'_{12}[\mathbf{v}]), |\mathbf{r}'_{12}[\mathbf{v}]|, 1), \text{AND}(\Re'_{12}[\mathbf{v}], -\mathbf{0}))); // (8)$ 
3   $\Im\hat{\mathbf{d}}_{22}^* = \text{DIV}(\Im'_{12}[\mathbf{v}], \text{MAX}(|\mathbf{r}'_{12}[\mathbf{v}]|, \mathbf{m})); // \text{from (8), here and above using (1)}$ 
4   $// \mathbb{R}: \Re\mathbf{d}_{22}[\mathbf{v}] = \text{AND}(\Re'_{12}[\mathbf{v}], -\mathbf{0}), \text{from (10), but only the sign bit (i.e., } \pm 0)$ 
5   $\Re'_{22}[\mathbf{v}] = \text{FMADD}(\Re''_{22}[\mathbf{v}], \Re\hat{\mathbf{d}}_{22}^*[\mathbf{v}], \text{MUL}(\Im'_{22}[\mathbf{v}], \Im\hat{\mathbf{d}}_{22}^*[\mathbf{v}])); // \text{and below from (8)}$ 
6   $\Im'_{22}[\mathbf{v}] = \text{FMSUB}(\Im''_{22}[\mathbf{v}], \Re\hat{\mathbf{d}}_{22}^*[\mathbf{v}], \text{MUL}(\Re'_{22}[\mathbf{v}], \Im\hat{\mathbf{d}}_{22}^*[\mathbf{v}])); // \text{Fused Mul and SUB}$ 
7   $// \mathbb{R}: \Re'_{22}[\mathbf{v}] = \text{XOR}(\Re''_{22}[\mathbf{v}], \Re\mathbf{d}_{22}[\mathbf{v}]), \text{from (10), but faster than multiplication}$ 
8   $\mathbf{r}_{22}[\mathbf{v}] = |\mathbf{r}'_{22}[\mathbf{v}]| = \text{HYPOT}(\Re'_{22}[\mathbf{v}], \Im'_{22}[\mathbf{v}]); // \mathbb{R}: \mathbf{r}_{22}[\mathbf{v}] = \text{ANDNOT}(-\mathbf{0}, \Re'_{22}[\mathbf{v}])$ 
9   $\Re\hat{\mathbf{d}}_{22} = \text{OR}(\text{MIN}(\text{DIV}(\text{ANDNOT}(-\mathbf{0}, \Re'_{22}[\mathbf{v}]), |\mathbf{r}'_{22}[\mathbf{v}]|, 1), \text{AND}(\Re'_{22}[\mathbf{v}], -\mathbf{0}))); // (9)$ 
10  $\Im\hat{\mathbf{d}}_{22} = \text{DIV}(\Im'_{22}[\mathbf{v}], \text{MAX}(|\mathbf{r}'_{22}[\mathbf{v}]|, \mathbf{m})); // \Im\hat{\mathbf{d}}_{22} = -\Im\hat{\mathbf{d}}_{22} \text{ implicitly; from (9)}$ 
11  $// \mathbb{R}: \Re\hat{\mathbf{d}}_{22}[\mathbf{v}] = \text{AND}(\Re'_{22}[\mathbf{v}], -\mathbf{0}), \text{from (10), but the sign bit extraction only}$ 

```

Fig. 9. Vectorized computation of $\tilde{\mathbf{D}}$, $\hat{\mathbf{D}}$, and \mathbf{R} from (8) and (9), or from (10).

```

1   $\mathbf{f} = \text{SET1}(1.34078079299425956\text{E}+154); // \sqrt{\text{DBL\_MAX}} \text{ from (14)}$ 
2   $\mathbf{x}[\mathbf{v}] = \text{MAX}(\text{DIV}(\mathbf{r}_{12}[\mathbf{v}], \mathbf{r}_{11}[\mathbf{v}]), \mathbf{0}); \mathbf{y}[\mathbf{v}] = \text{MAX}(\text{DIV}(\mathbf{r}_{22}[\mathbf{v}], \mathbf{r}_{11}[\mathbf{v}]), \mathbf{0}); // \text{see (13)}$ 
3   $\tan(2\varphi)[\mathbf{v}] = \text{OR}(\text{MIN}(\text{MAX}(\text{DIV}(\text{MUL}(\text{SCALEF}(\text{MIN}(\mathbf{x}[\mathbf{v}], \mathbf{y}[\mathbf{v}]), 1), \text{MAX}(\mathbf{x}[\mathbf{v}], \mathbf{y}[\mathbf{v}]))),$ 
4   $/* \text{from (14)} */ \text{FMADD}(\text{SUB}(\mathbf{x}[\mathbf{v}], \mathbf{y}[\mathbf{v}]), \text{ADD}(\mathbf{x}[\mathbf{v}], \mathbf{y}[\mathbf{v}], 1)), \mathbf{0}), \mathbf{f}), -\mathbf{0});$ 
5   $\tan\varphi[\mathbf{v}] = \text{DIV}(\tan(2\varphi)[\mathbf{v}], \text{ADD}(1, \text{SQRT}(\text{FMADD}(\tan(2\varphi)[\mathbf{v}], \tan(2\varphi)[\mathbf{v}], 1))));$ 
6   $\sec^2\varphi[\mathbf{v}] = \text{FMADD}(\tan\varphi[\mathbf{v}], \tan\varphi[\mathbf{v}], 1); \cos\varphi[\mathbf{v}] = \text{INVSQRT}(\sec^2\varphi[\mathbf{v}]); // \text{see (15)}$ 
7   $\tan\psi[\mathbf{v}] = \text{FMSUB}(\mathbf{y}[\mathbf{v}], \tan\varphi[\mathbf{v}], \mathbf{x}[\mathbf{v}]); \sec^2\psi[\mathbf{v}] = \text{FMADD}(\tan\psi[\mathbf{v}], \tan\psi[\mathbf{v}], 1);$ 
8   $\cos\psi[\mathbf{v}] = \text{INVSQRT}(\sec^2\psi[\mathbf{v}]); // \text{from (16) here and above}$ 
9   $\mathbf{c}_{\varphi}^{\psi}[\mathbf{v}] = \text{MUL}(\cos\varphi[\mathbf{v}], \cos\psi[\mathbf{v}]); \sigma'_{\max}[\mathbf{v}] = \text{MUL}(\text{MUL}(\mathbf{c}_{\varphi}^{\psi}[\mathbf{v}], \sec^2\psi[\mathbf{v}]), \mathbf{r}_{11});$ 
10  $\sigma'_{\min}[\mathbf{v}] = \text{MUL}(\text{MUL}(\mathbf{c}_{\varphi}^{\psi}[\mathbf{v}], \sec^2\varphi[\mathbf{v}]), \mathbf{r}_{22}); // \text{from (17) here and above}$ 

```

Fig. 10. Vectorization of the 2×2 SVD of a non-negative upper-triangular matrix from (13)–(17).

while the outputs are related to the quantities computed or implied in Fig. 10 as

$$\begin{aligned} \cos\varphi[\mathbf{v}] &= (\text{CSL}^{[k]})_k, & \cos\psi[\mathbf{v}] &= (\text{CSR}^{[k]})_k, & \sigma'_{\max}[\mathbf{v}] &= (\text{SSMAX}^{[k]})_k, \\ -\sin\varphi[\mathbf{v}] &= (\text{SNL}^{[k]})_k, & -\sin\psi[\mathbf{v}] &= (\text{SNR}^{[k]})_k, & \sigma'_{\min}[\mathbf{v}] &= (\text{SSMIN}^{[k]})_k. \end{aligned}$$

It is inadvisable to replace the vectorized algorithm in Fig. 10 by the DLASV2 calls, for at least two reasons. First, the input vectors have to be stored from the registers to the addressable memory. Then \mathbf{S} function calls have to be made instead of a single pass over the data, and the results finally have to be loaded from the memory into the vector registers for the last phase of the algorithm. Second, throughout the paper the tangents are used instead of the sines, to increase the accuracy by reducing the number of the roundings performed due to more opportunities for employing the fina-type operations [12]. However, DLASV2 provides the tangents only implicitly, as $\tan\beta = \sin\beta / \cos\beta$ for $\beta \in \{\varphi, \psi\}$. If the last phase of the algorithm comes after the DLASV2 calls, (29) has to be rewritten in the terms of

the respective sines to avoid the superfluous divisions, as the equivalent expressions

$$U = P_r \begin{bmatrix} d_{11}(\cos \alpha \cos \varphi - \hat{d}_{22} \sin \alpha \sin \varphi) & d_{11}(\cos \alpha \sin \varphi + \hat{d}_{22} \sin \alpha \cos \varphi) \\ -d_{22}(\sin \alpha \cos \varphi + \hat{d}_{22} \cos \alpha \sin \varphi) & d_{22}(\hat{d}_{22} \cos \alpha \cos \varphi - \sin \alpha \sin \varphi) \end{bmatrix}, \quad (31)$$

$$V = P_c \begin{bmatrix} \cos \psi & \sin \psi \\ -\tilde{d}_{22} \sin \psi & \tilde{d}_{22} \cos \psi \end{bmatrix}.$$

A quick test (albeit with computing $\tan \beta$ by two vector divisions for simplicity) has shown that an algorithm that calls DLASV2 as described is noticeably slower, more so in the real than in the complex (more involved in the other phases) case, relatively to the timings of the fully vectorized algorithm. Using DLASV2 instead of the method in Fig. 10 might therefore be a viable alternative only in the pointwise case, within a routine (e.g., `x1svd2`) designed in the LAPACK's style.

8. Numerical testing

All testing was performed on an Intel Xeon Phi 7210 CPU, running at 1.3 GHz with TurboBoost turned off in Quadrant cluster mode, with 96 GiB of RAM and 16 GiB of flat-mode MCDRAM (that was not used, since it is not available on the more recent generations of the Intel CPUs), under 64-bit CentOS Linux 7.8.2003.

The Intel C compiler, `icc` (version 19.1.1.217), was invoked with the following optimization and floating-point options: `-O3 -xHost -qopt-zmm-usage=high -fp-model source -no-ftz -prec-div -prec-sqrt -fimf-precision=high`, to enable the gradual underflow, prohibit the aggressive floating-point optimizations that could result in a loss of precision, and, together with `-fimf-use-svml=true`, to employ the high-accuracy SVML library. Among other options were `-std=c18` and `-qopenmp`. The DLASV2 routine was provided by the sequential Intel Math Kernel Library (MKL). The quadruple precision floating-point arithmetic, used for the error checking only, was supported by the `_float128` datatype and the functions operating on it, e.g., `_fmaq`, `_hypotq`, and `_scalbq`, with the obvious semantics.

The test data was harvested from `/dev/urandom` pseudorandom byte stream, with an approximately uniform probability distribution of each bit, and 64 consecutive bits formed a `double` precision value. A value that was not finite (either $\pm\infty$ or a NaN) was replaced with another one that was, sourced in the same way. In total 2^{36} finite doubles were stored in a binary file and reused for all runs. In the real case, the file layout was assumed to be a sequence of records, where each record contained four vectors (i.e., all the elements of $S \ 2 \times 2$ input matrices), as

$$\Re \mathbf{a}_{11}[\mathbf{v}], \Re \mathbf{a}_{21}[\mathbf{v}], \Re \mathbf{a}_{12}[\mathbf{v}], \Re \mathbf{a}_{22}[\mathbf{v}],$$

while in the complex case eight vectors were assumed per each record, as

$$\Re \mathbf{a}_{11}[\mathbf{v}], \Im \mathbf{a}_{11}[\mathbf{v}], \Re \mathbf{a}_{21}[\mathbf{v}], \Im \mathbf{a}_{21}[\mathbf{v}], \Re \mathbf{a}_{12}[\mathbf{v}], \Im \mathbf{a}_{12}[\mathbf{v}], \Re \mathbf{a}_{22}[\mathbf{v}], \Im \mathbf{a}_{22}[\mathbf{v}].$$

In both cases, a single batch comprised $n = \hat{n} = 2^{28}$ matrices—an absurdly large number for a typical usage scenario in the $2n \times 2n$ SVD algorithm, but necessary

for a reliable timing of each batch, to compensate for the unavoidable operating system's jitter. Therefore, in the real case the test file contained 64 batches, and the same file provided 32 batches in the complex case. Execution of each batch by the parallel for loop from Fig. 2 with 32 OpenMP threads, spread across the 64 CPU cores such that each thread was affinity-bound to its own core while no two threads shared the same level-2 cache, resulted in the following summary outputs:

1. the wall time t in seconds for processing the entire batch, measured by placing the `omp_get_wtime` calls immediately before and after the aforesaid parallel loop,
2. the maximal *a posteriori* spectral condition number of the matrices in the batch,

$$\kappa = \max_{1 \leq k \leq n} \kappa_2(\mathbf{A}^{[k]}) = \text{fmin}(\sigma_{\max}^{[k]}/\sigma_{\min}^{[k]}, \infty), \quad (32)$$

3. the maximal normwise relative error of the singular value decompositions, as

$$\rho = \max_{1 \leq k \leq n} \text{fmax}(\|\mathbf{U}^{[k]}\mathbf{\Sigma}^{[k]}(\mathbf{V}^{[k]})^* - \mathbf{A}^{[k]}\|_F / \|\mathbf{A}^{[k]}\|_F, 0), \quad (33)$$

4. the maximal departure from orthogonality of the left singular vectors, as

$$\delta = \max_{1 \leq k \leq n} \|(\mathbf{U}^{[k]})^* \mathbf{U}^{[k]} - \mathbf{I}\|_F, \quad (34)$$

5. and the maximal departure from orthogonality of the right singular vectors, as

$$\eta = \max_{1 \leq k \leq n} \|(\mathbf{V}^{[k]})^* \mathbf{V}^{[k]} - \mathbf{I}\|_F. \quad (35)$$

The last four metrics above (κ , ρ , δ , and η) were computed after the batch had been entirely processed and the output data had been converted to quadruple precision by the value-preserving casts. The results were then printed out by rounding them first to the hardware's 80-bit extended datatype (`long double`, with a negligible error), while the timings were rounded to the nearest microsecond.

The pointwise algorithm was implemented in the real (`d1svd2`) and the complex (`z1svd2`) variant. The first two phases of the pointwise algorithm are arithmetically equivalent to those of the vectorized one if the scalar hypot and invsqrt functions are equivalent to the respective vector ones, in an arbitrary lane. The SVD of a non-negative upper-triangular matrix was performed in the pointwise algorithm by a single `DLASV2` call (see section 7), and the subsequent formation of U and V was done as in (31), to compare the accuracy (i.e., ρ , δ , and η) of such an approach with the one proposed for the vectorized algorithm. Also, the pointwise implementations in C are as close as possible to the LAPACK-style Fortran routines that could be written for this specific purpose of computing the general 2×2 SVD, without any of the overhead a call to an $m \times n$ SVD routine would necessarily incur, thus allowing a fair comparison of the execution times, as follows. Each call to `dSsvd2` or `zSsvd2` was replaced by S calls (one for each of the argument vectors' lanes) to `d1svd2` or `z1svd2`, respectively, and the rest of the testing code (i.e., the batch timing and the error checking parts) was left intact. The speedup is a ratio of the wall time required for processing a batch with the pointwise algorithm so employed and the wall time required for the same job using the vectorized algorithm as proposed.

The maximal condition number κ from (32) attained in the real case varies from one batch to another, from $4.447666 \cdot 10^{617}$ to $2.134020 \cdot 10^{620}$, and in the complex case from $6.545644 \cdot 10^{614}$ to $9.167483 \cdot 10^{616}$, so in each batch there was at least one almost as highly ill-conditioned matrix as possible, without being exactly singular.

Fig. 11 shows the attained speedup. In the real case, the wall times t vary from 5.767176 s to 5.793884 s for the vectorized algorithm, and from 21.611207 s to 21.993982 s for the pointwise one. In the complex case, the ranges are 18.844251 s to 19.234680 s, and 54.771144 s to 55.227508 s, respectively. Being somewhat more (in the real case) or less (in the complex case) than three times, the speedup has thus justified the purpose of designing the vectorized algorithm, but also suggests that the pointwise algorithm should be used instead when n equals one or two.

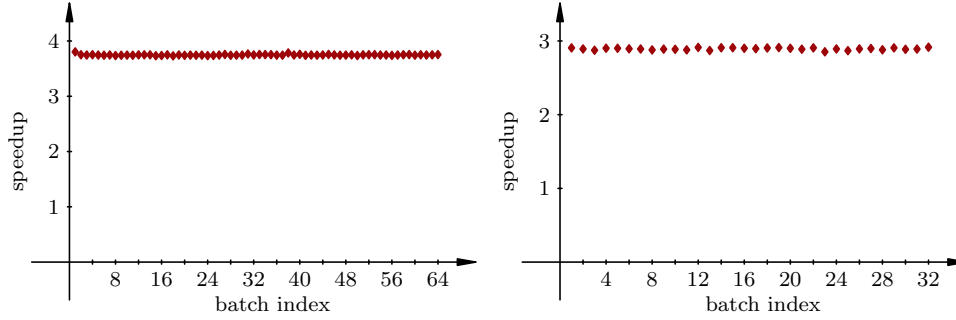


Fig. 11. The speedup attained with each batch processed by the vectorized algorithm (`xSsvd2`) vs. the pointwise algorithm (`x1svd2`), in the real ($x = d$, left) and the complex ($x = z$, right) case.

Fig. 12 shows that for the vast majority of batches, the vectorized algorithm gives a bit more accurate decomposition than the pointwise one, but both are usable. The optional backscaling was proven to be unsafe, since in each batch at least one singular value overflowed when backscaled, with either algorithm and in either case.

Figs. 13 and 14 demonstrate that the vectorized algorithm generally results in the more orthogonal left and right singular vectors, respectively, than the pointwise one, since there is less rounding involved in computing the vectors in the former.

9. Conclusions

This paper has shown that a batched computation of the SVDs of order two can be vectorized with a relative ease on the Intel AVX-512 architecture. Other vectorization platforms might be targeted as well, if they provide the instructions analogous to those required here. Single precision could be used instead of double precision.

Compared to the pointwise processing of one matrix at a time, the vectorized algorithm is nearly or more than three times faster, in the complex and the real case, respectively, and generally slightly more accurate when computing the SVDs of

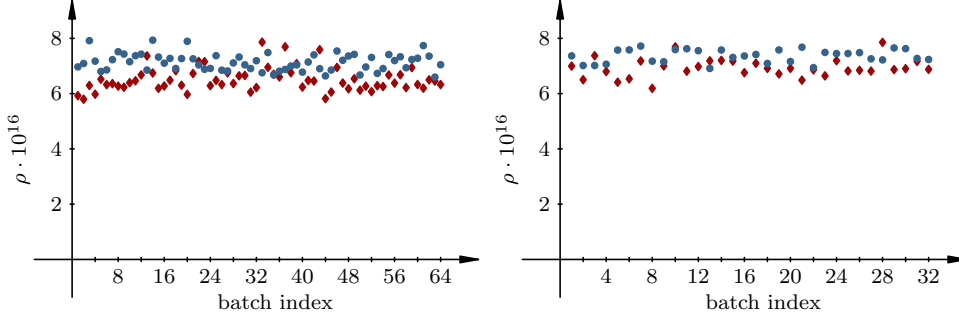


Fig. 12. The maximal normwise relative errors ρ from (33) for each batch processed by the vectorized (♦) and the pointwise (•) algorithm, in the real (left) and the complex (right) case.

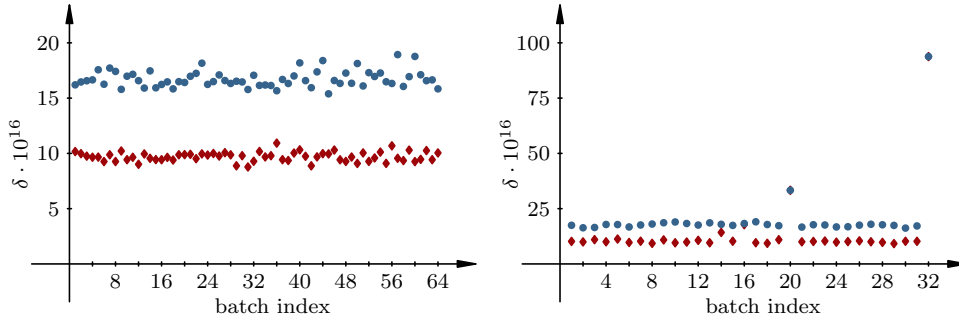


Fig. 13. The maximal departures from orthogonality δ from (34) for each batch processed by the vectorized (♦) and the pointwise (•) algorithm, in the real (left) and the complex (right) case.

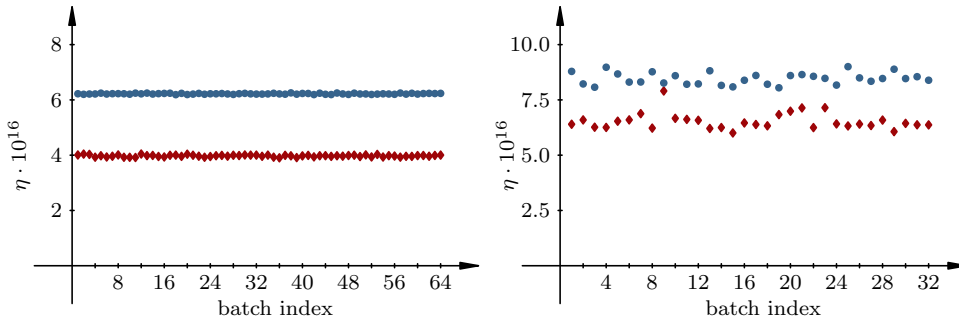


Fig. 14. The maximal departures from orthogonality η from (35) for each batch processed by the vectorized (♦) and the pointwise (•) algorithm, in the real (left) and the complex (right) case.

non-negative upper-triangular matrices as proposed versus the standard procedure of DLASV2. Additionally, the exact scalings of the input matrices ensure that the scaled singular values never overflow, provided that the input elements are all finite.

A similar vectorization principle, relying on a vector-friendly data layout (see section 3), could be applied to the various algorithms for factorizations or decompositions of a batch of matrices of a small, fixed order, if the control flow within the algorithm can be transformed into a branch-free one, as it has been done here for the column and the row pivotings in section 6, and for handling the special values.

Acknowledgements

This work has been supported in part by Croatian Science Foundation under the project IP-2014-09-3670 “Matrix Factorizations and Block Diagonalization Algorithms” (MFBDA).

The author would like to thank Sanja Singer for her assistance in preparation of Figs. 11, 12, 13, and 14 with METAPOST.

References

- [1] E. G. Kogbetliantz, Solution of linear equations by diagonalization of coefficients matrix, *Quart. Appl. Math.* **13**(2) (1955) 123–132.
- [2] M. Bečka, G. Okša and M. Vajteršić, Dynamic ordering for a parallel block-Jacobi SVD algorithm, *Parallel Comp.* **28**(2) (2002) 243–262.
- [3] G. Okša, Y. Yamamoto, M. Bečka and M. Vajteršić, Asymptotic quadratic convergence of the two-sided serial and parallel block-Jacobi SVD algorithm, *SIAM J. Matrix Anal. and Appl.* **40**(2) (2019) 639–671.
- [4] V. Novaković and S. Singer, A Kogbetliantz-type algorithm for the hyperbolic SVD, arXiv:2003.06701 [math.NA] (March, 2020).
- [5] ISO/IEC JTC1/SC22/WG14, *ISO/IEC 9899:2018(en) Information technology — Programming languages — C*, 4th edn. (ISO, 2018). International standard.
- [6] Intel Corporation, *Intel® 64 and IA-32 Architectures Software Developer’s Manual* (October, 2019). <https://software.intel.com/en-us/articles/intel-sdm> (Order No. 325462-071US, Combined Volumes: 1, 2A, 2B, 2C, 2D, 3A, 3B, 3C, 3D and 4).
- [7] S. Singer, E. Di Napoli, V. Novaković and G. Čaklović, The LAPW method with eigendecomposition based on the Hari–Zimmermann generalized hyperbolic SVD, arXiv:1907.08560 [math.NA] (July, 2019).
- [8] V. Hari, On the global convergence of the complex HZ method, *SIAM J. Matrix Anal. Appl.* **40**(4) (2019) 1291–1310.
- [9] V. Hari, Globally convergent Jacobi methods for positive definite matrix pairs, *Numer. Algorithms* **79** (Sep 2018) 221–249.
- [10] V. Novaković, S. Singer and S. Singer, Blocking and parallelization of the Hari–Zimmermann variant of the Falk–Langemeyer algorithm for the generalized SVD, *Parallel Comput.* **49** (2015) 136–152.
- [11] V. Novaković, Parallel Jacobi-type algorithms for the singular and the generalized singular value decomposition, PhD thesis, University of Zagreb, Croatia (<https://urn.nsk.hr/urn:nbn:hr:217:515320>, December 2017)
- [12] Z. Drmač, Implementation of Jacobi rotations for accurate singular value computation in floating point arithmetic, *SIAM J. Sci. Comput.* **18**(4) (1997) 1200–1222.
- [13] V. Hari, S. Singer and S. Singer, Block-oriented J -Jacobi methods for Hermitian matrices, *Linear Algebra Appl.* **433**(8–10) (2010) 1491–1512.
- [14] V. Hari, S. Singer and S. Singer, Full block J -Jacobi method for Hermitian matrices, *Linear Algebra Appl.* **444** (2014) 1–27.

- [15] A. Haidar, A. Abdelfattah, M. Zounon, S. Tomov and J. Dongarra, A Guide for Achieving High Performance with Very Small Matrices on GPU: A Case Study of Batched LU and Cholesky Factorizations, *IEEE Trans. Parallel Distrib. Syst.* **29**(5) (2018) 973–984.
- [16] J. Dongarra, M. Gates, J. Kurzak, P. Luszczek and Y. M. Tsai, Autotuning Numerical Dense Linear Algebra for Batched Computation With GPU Hardware Accelerators, *Proc. IEEE* **106**(11) (2018) 2040–2055.
- [17] G. W. Stewart, An updating algorithm for subspace tracking, *IEEE Trans. Signal Process.* **40**(6) (1992) 1535–1541.
- [18] J. P. Charlier, M. Vanbegin and P. Van Dooren, On efficient implementations of Kogbetliantz’s algorithm for computing the singular value decomposition, *Numer. Math.* **52**(3) (1987) 279–300.
- [19] V. Hari and J. Matejaš, Accuracy of two SVD algorithms for 2×2 triangular matrices, *Appl. Math. Comput.* **210**(1) (2009) 232–257.
- [20] J. Matejaš and V. Hari, On high relative accuracy of the Kogbetliantz method, *Linear Algebra Appl.* **464** (2015) 100–129.
- [21] E. Anderson, Z. Bai, C. Bischof, S. Blackford, J. Demmel, J. Dongarra, J. Du Croz, A. Greenbaum, S. Hammarling, A. McKenney and D. Sorensen, *LAPACK Users’ Guide*, 3rd edn. (Society for Industrial and Applied Mathematics, Philadelphia, PA, USA, 1999).
- [22] S. Qiao and X. Wang, Computing the Singular Values of 2-by-2 Complex Matrices, <http://www.cas.mcmaster.ca/sqrl/papers/sqrl5.pdf> (May, 2002).
- [23] IEEE Task P754, *IEEE 754-2008, Standard for Floating-Point Arithmetic* (IEEE, New York, NY, USA, August 2008).
- [24] NVIDIA Corporation, *CUDA C++ Programming Guide v10.2.89* (November, 2019). <https://docs.nvidia.com/cuda/cuda-c-programming-guide/>.
- [25] V. Novaković and S. Singer, An implicit Hari–Zimmermann algorithm for the generalized SVD on the GPUs, arXiv:1909.00101 [math.NA] (August, 2019).
- [26] OpenMP Architecture Review Board, *OpenMP Application Programming Interface Version 4.5* (November, 2015). <https://www.openmp.org/wp-content/uploads/openmp-4.5.pdf>.